

CHARACTERIZATION AND DFN MODELLING OF THE FRACTURE NETWORK IN A MESOZOIC KARST RESERVOIR: GOMBA OILFIELD, PALEOGENE BASIN, CENTRAL HUNGARY

M. Bauer^{1*} and T. M. Tóth²

Reservoir rocks at Gomba oilfield, located in the Hungarian Paleogene Basin, include fractured and karstified Triassic carbonates with significant fluid storage potential. However little information is available about the fracture network in these carbonates which has led to production problems at Gomba. The purpose of this study is to investigate the relationship between the spatial distribution of high porosity zones in the carbonates and the micro-fracture system. For this evaluation, individual fractures were studied and used in a discrete fracture network (DFN) modelling exercise at two wells, Gomba-1 and Gomba-3. The investigation took place at two different scales. Fracture length and aperture distributions were derived at the micro-scale (mm to cm), whereas fracture density and fracture orientation data were investigated at the reservoir scale. The results of both investigations were taken into consideration in the modelling. The results of the fracture network models were compared to reservoir lithologies which ranged from fractured carbonates to collapse breccias.

Based on the results, it appears that the porosity associated with a significant proportion of the fractures was increased as a result of dissolution. Fracture distribution was not uniform along the studied well paths, and fracture orientation was chaotic at particular depth intervals. On the basis of the DFN models, three different fractured zones are predicted to occur in the reservoir, but only two of the zones have significant fracture porosity.

Comparing these results with petrographic observations, an epigene karst phase is proposed which is older than (or the same age as) the time of hydrocarbon migration; karst-related voids were therefore important pathways for fluid migration. The void system and karst caverns partly collapsed during subsequent burial, resulting in karst-related traps. By analogy with modern cave systems, the karst cavern zones at Gomba probably extend horizontally rather than vertically, and are oriented NE-SW parallel to major structural lineaments.

INTRODUCTION

The relationship between fracture systems in limestone bodies and karst phenomena has been analyzed in numerous studies (e.g. Palmer, 1991; Gabrovšek and Dreybrodt, 2001; Kaufmann, 2003a). These studies

¹ University of Szeged, Department of Mineralogy, Geochemistry and Petrology, Geological and Geophysical Institute of Hungary, H-6722, Szeged, Egyetem St 2, Hungary.

² University of Szeged, Department of Mineralogy, Geochemistry and Petrology, Szeged, Hungary.

*Author for correspondence: bauer.marton@mfgi.hu

Key words: Palaeokarst, fractures, carbonates, DFN modelling, Hungary, Paleogene Basin, Gomba field.

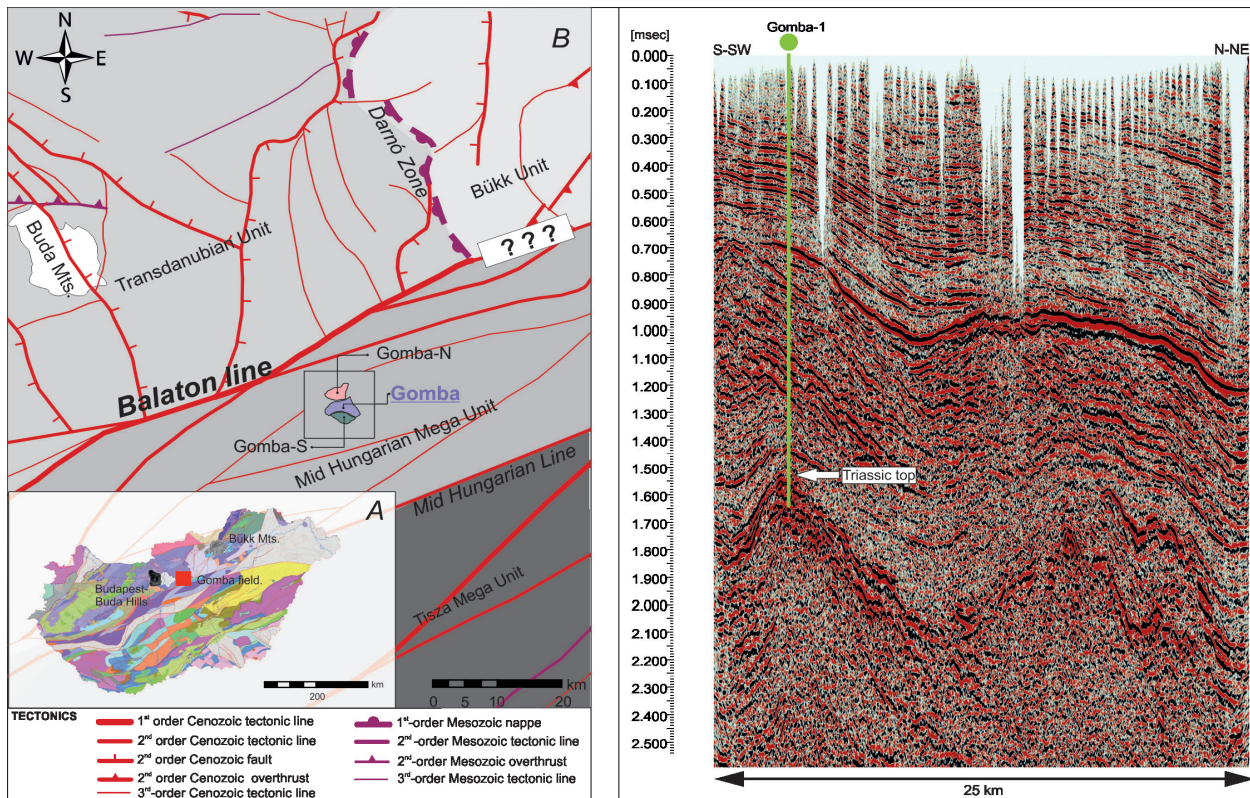


Fig. 1. (left) Pre-Cenozoic basement map of the area around Gomba field in the Paleogene Basin, Hungary (based on Haas *et al.*, 2010). Structural lineaments and faults are shown. ??? indicates the uncertain southern margin of the Bükk Unit. Inset map shows Mesozoic basement units (purple, blue and light green). (right) NNE-SSW oriented seismic line passing through the Gomba-I well showing the “buried hill” structure at Gomba field.

suggest that a close correlation exists between the connectivity and permeability of a fracture network and the intensity of dissolution occurring along the fractures; more intense dissolution takes place in more permeable zones (Singurindy and Berkowitz, 2005). In karstified carbonate reservoir rocks, this relationship is of fundamental importance in terms of palaeo-fluid migration and may control the spatial configuration of dissolution features (Palmer, 1991; Diabat, 2013; Bauer and M.Tóth, 2015). Thus if the fracture network can be characterized, this information can be used to investigate the influence of karst or palaeokarst phenomena. In addition, other features of karstified reservoir carbonates which need to be evaluated include the location of dissolved and cemented fractures, palaeo-cave collapse structures, and features which may be “invisible” in seismic data (e.g. small cave systems, shafts) but which may have had a considerable impact on fluid migration.

A significant proportion of fields in the Hungarian Paleogene Basin produce from fractured and karstified carbonates. In fractured/karstified systems, hydrocarbons in general migrate along pathways which are associated with secondary (fracture) and perhaps tertiary (karst-related) porosity (Reimann *et al.*, 2014; Karay and Hajnal, 2015). However, the

spatial distribution of karst-related voids is mainly controlled by structural deformation, i.e. by fracture and fault systems (Jeannin, 1990; Benkovics *et al.*, 1999; Hauselmann *et al.*, 1999).

At the Gomba field (Fig. 1), the main reservoir units are fractured and brecciated Triassic limestones of the Kisfennsík or Berva Formation, and basal Eocene siliciclastics of the Kosd Formation. The Triassic limestones were karstified during the Paleogene as shown by studies of outcrops in the Bükk Mountains (Pelikán, 2005) and were subsequently buried during the Neogene, which probably resulted in the development of features including collapse breccias (Bauer *et al.*, 2016).

Collapse zones in karstified carbonates in general have a brecciated central “core” which is commonly enveloped by a fractured “disturbed zone” (Loucks, 1999). Benedek (2009) and Bauer *et al.* (2016) described polymictic breccias in cores from the Gomba field and interpreted them as karst-related breccias or cave sediments, but the spatial distribution of the disturbed zones is not well known. Bauer *et al.* (2016) identified four generations of fractures in Triassic carbonates at Gomba based on petrographic and microtextural features. Three of the fracture generations were interpreted to be older than the

karst-related breccia, and the fourth was interpreted to be younger.

One object of this study is to investigate whether there were particular zones within the carbonate reservoir succession at Gomba where the conditions were more favorable for cave formation than elsewhere. An additional aim is to investigate the possible relationship between the micro-fracture system and the reservoir lithologies. We attempt to quantitatively investigate individual fractures, analyze their geometric aspects, and scale-up the results to better understand the effects of the fracture pattern and the associated dissolution on fluid migration pathways.

Geological background

The Gomba field is one of the most important oil fields in Hungary and was first drilled by MOL PLC in 2003. However in spite of the long production history, the petrology and microstructure characteristics of the carbonate reservoir rocks are poorly known. The field is located in the Hungarian Paleogene Basin (Fig. 1a), an elongate basin which evolved during the Paleocene and Eocene as part of the Central Paratethys basin system (Popov, 2004). Gomba field is located in the southern Buda Paleogene Unit which is located in the northern part of Central Hungary.

Seismic data show that the field is crossed by two significant fault systems, the Balaton Line and the Mid-Hungarian Line (Fig. 1). The Balaton Line is the eastern continuation of the Peri-Adriatic Lineament which separates the Eastern and Southern Alps. The Mid-Hungarian Line is a major structure in the Intra-Carpathian area (Géczy, 1973; Kázmér and Kovács, 1985; Csontos *et al.*, 1992; Fodor *et al.*, 1992, 1998; Csontos and Nagymarossy, 1998; Palotai and Csontos, 2010). The complex structural history of the Gomba area includes Oligocene – early Miocene thrusting, middle Miocene extension, local late Miocene inversion and late Miocene – Pliocene normal faulting, as well as left-lateral wrenching (Csontos and Nagymarossy, 1998).

Gomba field produces from karstified Triassic carbonates in a “buried hill” structure a depth of about 2500 m below the present-day surface (Fig. 1b); the structure is surrounded by deep synclinal troughs filled with Paleogene and Neogene siliciclastics. Hydrocarbons at Gomba are generated by the Paleogene Petroleum System, one of six recognized in the Pannonian Basin Province (Dolton, 2006). In the Paleogene Petroleum System, source rocks are composed of the euxinic Tard Clay (upper Eocene to lower Oligocene) and the Kiscell Clay (lower Oligocene) (Fig. 2a). In northern Hungary these anoxic clays have an average TOC content of 0.5–1.0%, locally as high as 4.5% (Kókai, 1994; Milota *et al.*, 1995). Kerogen is mostly Type I and II, but Type III

kerogen is present in the upper part of the sequence (Dolton, 2006).

The main reservoir units at Gomba are the basal Paleogene – Lutetian siliciclastics of the Kosd Sandstone and the Triassic Kiszfennsík or Berva Limestones (Benedek, 2009; Bauer *et al.*, 2016) (Fig. 2a) which are separated by a major unconformity recognised throughout the Paleogene Basin. The Kosd Formation consists of red and yellow clays, sands, gravels, and dolomite and limestone debris (Less, 2005) and extends over much of northern Hungary. The Kiszfennsík Limestone is comparatively poorly known and at the surface has only been described in the Bükk Mountains in the Inner Western Carpathians; its westernmost occurrence is in the subsurface at Gomba field (Benedek, 2009; Bauer *et al.*, 2016). At Gomba it is in general composed of pale grey limestones interpreted to have been deposited in tidal flat, lagoonal and shallow-marine environments. Limestones are mainly thick-bedded or massive and contain subordinate thinly-bedded intervals, locally with fenestral fabrics (Bauer *et al.*, 2016). Syngenetic brecciation occurs quite frequently (Pelikán, 2005).

Seven wells in the Gomba field penetrated the Kiszfennsík Formation which, based on core and thin-section observations, is composed of partly dolomitized grainstones and packstones including oncoids and peloids (Fig. 2b) with a negligible clay content (Bauer *et al.*, 2016). The carbonates are in general strongly fractured. Well logs indicate that the upper few tens of metres of Triassic limestones at the Triassic/Eocene unconformity have significant porosity and permeability. However, it was not possible to obtain core samples from this zone because of total mud loss during drilling (yellow stars, Fig. 2a). The closest cores to the unconformity consist of polymictic breccias which have been interpreted to result from hydrofracturing and palaeo karst-related processes (Bauer *et al.*, 2016), or as a regolith similar to that recognized in the Buda Mountains (c.f. Nádor, 1993). Similar polymictic breccias occur in deeper parts of the reservoir and are interpreted as palaeo-karst breccias, collapse breccias and/or palaeo-cave sediments (Bauer *et al.*, 2016).

Both non-brecciated and brecciated intervals are heavily fractured as indicated by FMI and CBIL (acoustic borehole televiewer) data and available cores (Benedek, 2009). Microstructural evaluation of the core material indicated four separate fracture generations, three of which are completely filled with calcite cement. Thus three fracture sets were formed before brecciation and epigene karstification, while the final set developed during or after these processes (Bauer *et al.*, 2016). The youngest fracture generation is partly filled with calcite cement but it also contains free storage capacity. According to the model presented

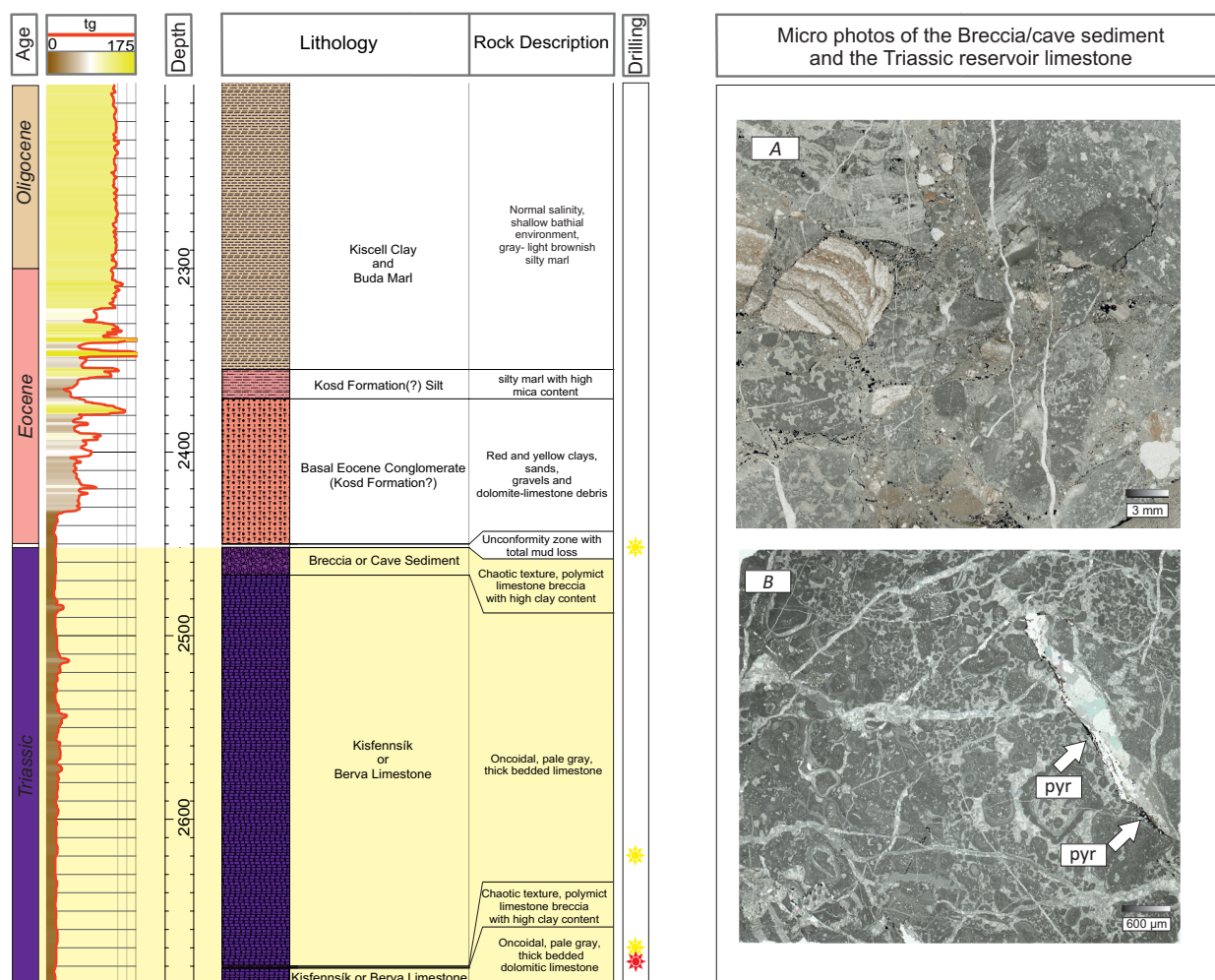


Fig. 2 (left) Generalized lithostratigraphic column for the Gomba-I borehole with the total gamma log (left), and showing intervals with significant mud loss (yellow stars) and the depth at which the drill bit blew-off (red star) (wireline logs were recorded by MOL PLC; Benedek 2009). For details, see text. **(right)** Photomicrographs of the Triassic Kisfennsík Formation carbonates showing (A) the typical texture of the polymict breccia interpreted as a palaeo cave sediment, and (B) an oncoidal limestone (pyr: pyrite).

by Benedek (2009), hydrocarbons may have migrated into the Eocene reservoir rocks through the Triassic carbonates because the porosity and permeability of the limestone is higher than that of the overlying strata in the adjacent sedimentary troughs (see Fig. 1). Thus the final fracture generation has been an active migration pathway, and migration continues at the present day.

The reservoir at Gomba field is compartmentalized and three sectors are recognized: Gomba-North, Gomba and Gomba-South (Fig. 1a). Gomba-North has a different, higher density type of oil than the central Gomba and Gomba-South sectors, for reasons which are not understood.

METHODS

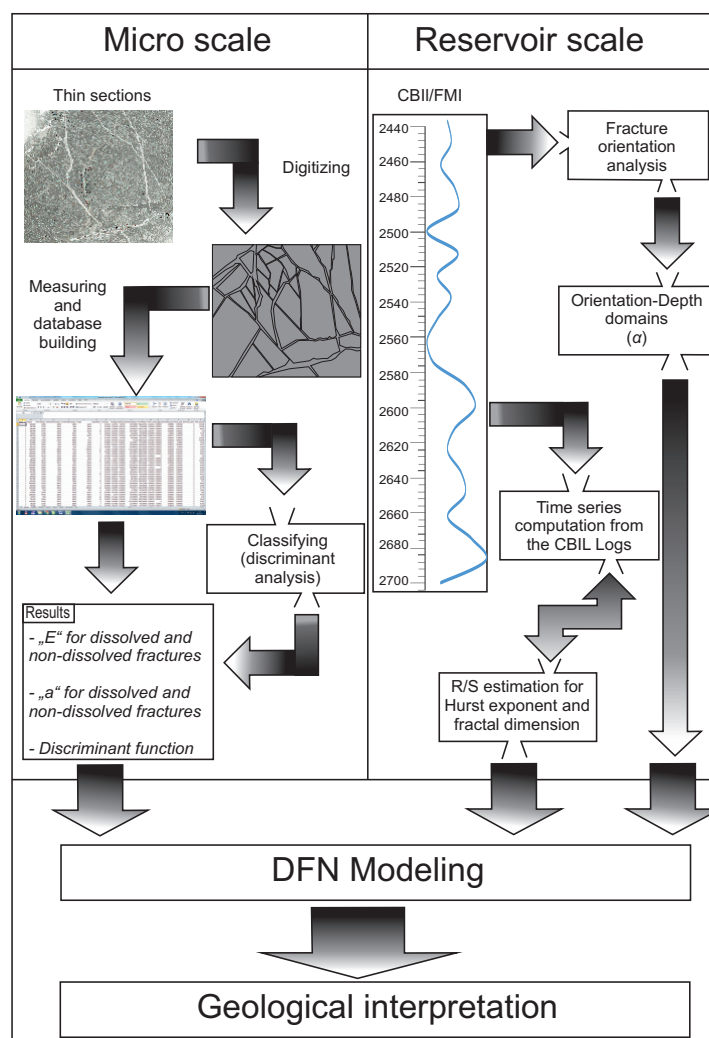
Various well-logging methods can be used to measure the position and orientation of fractures but are not able to characterize them in terms of qualitative parameters such as fracture shape and connectivity relationships. These parameters can however be derived from thin

sections or digitized core images. Therefore, in order to characterize the fracture network in the Triassic carbonates studied, data were collected at two scales. Fracture shape was analyzed in thin sections, while other quantitative data (such as fracture density and orientation) was analyzed at the well-log scale. Both data sets were then used to build an integrated discrete fracture network (DFN) model (Fig. 3).

Micro-scale studies

Twenty-one polished thin sections (5 x 5 cm²) were prepared from samples of Triassic reservoir carbonates from the Gomba-1, Gomba-3 and Gomba-6 wells from different depths. The samples consisted of non-brecciated limestone (n = 17) and polymictic limestone breccia (n = 4). Input files for image analysis were recorded with an Epson X6000 scanner in plane-polarised light at 6000 dpi resolution. The digital images were then traced manually on-screen in CorelDraw to delineate fracture types, and the traced images were analyzed using ImageJ software (Rasband,

Fig. 3. Workflow for DFN modelling and interpretation. See text for details.



1997-2006); in addition Olympus Stream Essential 1.9 was used to calculate geometric parameters.

During the image analysis, fractures were classified into two types – dissolved and non-dissolved – from the shape of the fracture walls. Fracture walls with a purely structural origin usually have simple shapes which become more complex as a result of dissolution (Feng *et al.*, 2013). Thus the simplest-shaped fractures were assigned to the “non-dissolved” (structural) category, while more complex fractures were assigned to the “dissolved” category. A transitional category contains fractures which were neither clearly dissolved nor non-dissolved.

Measured parameters

Basic geometric parameters including fracture area (A), perimeter (P) and length (L) were measured on the thin sections, and the elongation (E) was determined (see abbreviations and definitions in Table 1). Other geometric features were also measured accurately to differentiate dissolved and non-dissolved fracture types such as convexity (C), roundness (R), aspect ratio (AR), Feret diameter (F, *see below*) and sphericity (S)

The fracture length distribution was calculated independently for the non-brecciated limestone and for breccia reservoir rocks. Only those fractures were involved in the analysis which terminated inside the studied core sample.

Fracture lengths in general have a non-symmetrical frequency distribution and there are more small fractures than large ones. Thus a power-law relationship (Yielding *et al.*, 1992; Min *et al.*, 2004) of the general form

$$N(L) = F \cdot L^{-E} \quad (1)$$

best describes the fracture-length frequency distribution. Because the number of classes in the frequency distribution function (k) may influence the shape of the histogram, this number was defined as

$$k = 2 * \text{INT}(\log_2(\max(L))) \quad (2)$$

prior to fitting the analytical curve. The truncation effect was also taken into consideration during the calculation.

Table 1. Abbreviations and definitions of the geometric parameters used.

Abbreviation	Name	Definition/ formula
α, β	fracture orientation	dip, dip direction
a	aperture	Mean of diameter and Feret diameter
A	area	The number of pixels covering the area
P	perimeter	Number of pixels in the perimeter
L	length	Number of pixels in a line
C	convexity	Total area divided by the convex area of the measured object
S	sphericity	\sim square of the ratio of width and length
F_{min}	minimum Feret diameter	F_{min} is the shortest distance between parallel tangents touching opposite sides of the fracture wall
F_{max}	maximum Feret diameter	F_{max} is the greatest distance between parallel tangents touching opposite sides of the fracture wall, also known as the maximum caliper length
PA	perimeter/area	$PA = \frac{\text{perimeter}}{\text{area}}$
R	roundness	$R = 4 * \frac{\text{area}}{\pi * \text{major axis}^2}$
AR	aspect ratio	$AR = \frac{\text{minor axis length}}{\text{major axis length}}$
E	elongation	$E = \frac{\text{longest distance from the centre}}{\text{shortest distance from the centre}}$
D	fractal dimension	box-counting method
E	exponent of length distribution	$N=(L)F*L^{-E}$

Measurement of the fracture aperture is not straightforward. In many cases, the distance between opposing fracture walls could not be measured accurately because of the irregular nature and roughness of the walls. A frequently applied method is to measure the aperture at three different points (or more, typically four or five), and to identify a geometric parameter which describes the aperture in 2D. This parameter is known as the Feret diameter (Feret, 1931) and defines the distance between two parallel tangential lines rather than between the walls. In this paper, aperture (a) is therefore defined as the average of the minimum Feret (F_{min}) and maximum Feret (F_{max}) diameter values.

Data processing

Data processing began with analyzing outliers in the data set. Outliers originate for example if fracture size is smaller than the detection limit, or if fracture length exceeds the dimensions of the thin section. The outliers were extracted by box-plot charts of the area parameter in SPSS 22.0 software.

Characterization of the dissolution state of the individual fractures was computed by discriminant

function analysis. During this statistical approach, Wilk's lambda step-wise method of regression analysis was applied (Nath and Pavur, 1985). The grouping variable was the classification category (dissolved or non-dissolved), and the independent variables were the measured parameters in addition to the following calculated variables: diameter/area, (Feret diameter / area) *100, Feret diameter / diameter, perimeter / sphericity, elongation / perimeter, aspect ratio / perimeter, aspect ratio / area, and Feret diameter / perimeter (see Table 1 for details).

Reservoir scale studies

The wells investigated were not drilled with core recovery over the full length of the borehole. Therefore, even if the digitized thin sections were able to characterize the fracture network to a high resolution, they only represent portions of the reservoir over only a few tens of metres. To analyze the entire fracture network, CBIL and FMI log data were used to calculate the fracture density and to describe the fracture orientation (dip and dip angle). Orientation values for the fracture network modelling were derived directly from the FMI logs.

Well-log methods have frequently been used to study fractured reservoirs (e.g. Bean, 1996; Marsan and Bean, 1999) because they provide valuable information at the reservoir scale. Borehole image logs (e.g. FMI) and various core imaging processes result in deterministic data sets concerning fractures with exact spatial positions (Tezuka and Watanabe, 2000; Yang *et al.*, 2004). The intersection points between the fracture network and the borehole can be analyzed mathematically as a time series which can be characterized by its Hurst exponent (H), from which the fractal dimension (D) of the fracture network can be calculated (M.Tóth, 2010).

In this study, H values were calculated by using R/S analysis in Benoit 1.0 software. Based on the H values estimated for a series at least 200 points, the fractal dimension of fracture mid-points can be computed by using a simple linear equation (M.Tóth, 2010). In this way, variations in fracture density (measured as the fractal dimension) along the well can be determined. Mathematical aspects of fracture density estimation using well-log data were discussed in more detail by M.Tóth (2010).

Fracture network simulation

Analysis of the geometric parameters of the fracture sets allowed a discrete fracture network (DFN) to be simulated for the study area. Numerous DFN simulators are available (e.g. FracMan, RMS, and Connect Flow). The RepSim code was used here and has previously been applied to solve 3D fracture network simulation problems (M.Tóth *et al.*, 2004; Vass *et al.*, 2009; Bauer and M.Tóth, 2015). One significant difference among the DFN simulation software programmes concerns the fracture centre allocation. Many programs allocate the fracture centres uniformly (e.g. Dershowitz and Einstein, 1988) or following a Poisson point process (Priest and Hudson, 1976), while others take into consideration the scale invariance of the fracture networks and allocate the fracture centres with a given fractal dimension (e.g. Hewett, 1995). The RepSim code is based on fractal geometry. It follows the box-counting algorithm to locate fracture mid-points in 3D using the calculated value of D, the fractal dimension, while elongation and orientation data are used to generate the surrounding fracture network. By evaluating the simulated fracture network, this code can also be used to calculate the spatial position of the interconnected fracture sets.

RESULTS

Micro-scale results

Fracture geometry

Individual fractures ($n = 152$) were evaluated using the methods described above. Most records represent

fractures in non-brecciated limestone which were much more intensely fractured than the brecciated limestones. Fractures in breccia are mostly present within individual limestone clasts, although locally the youngest fracture generation (F4 of Bauer *et al.*, 2015) cross-cuts both the matrix and the clasts. Histograms of measured fracture parameters such as area, aspect ratio and elongation (Fig. 4B/1-3) show that there was little significant difference in the fracture geometry between dissolved and non-dissolved limestones, and fractures in the different rock types are therefore not distinguished hereafter.

A number of quantitative differences between non-dissolved and dissolved fractures (Fig. 4 A) were recorded. One of the most prominent differences concerns the logarithm of area. Thus dissolved fractures have much larger areas in 2D than non-dissolved fractures (Fig. 4 B/1). There are also significant differences in aspect ratio (Fig. 4 B/2), elongation (Fig. 4 B/3) and convexity; all of these variables have much smaller values for non-dissolved fractures. The values of the ratios of elongation/Feret diameter and $\ln(\text{Feret})$ diameter are higher for dissolved fractures than for non-dissolved fractures. Sphericity values do not show any significant difference between different fracture types.

Fracture type classification

Based on these observations, a classification function was computed to characterize and distinguish dissolved and non-dissolved fractures. During the digitization, 72 cases were clearly identified as dissolved fractures, 64 as non-dissolved fractures, and 16 were not classified. As a result of the discriminant function analysis, the main classifying parameters were found to be PA, C, S, $\ln(L)$, $\ln(P)$ and $\ln(F_{\min})$ (abbreviations in Table 1) in the following unstandardized discriminant function:

$$F(D) = 72.6 \text{ PA} + 15.17 \text{ C} + 9.4 \text{ S} + 5 \text{ P} + 4.1 \text{ L} - 2.2 \text{ A} - 4.2 \text{ F}_{\min} - 40.88 \quad (3)$$

On the basis of this function, dissolved and non-dissolved fractures could clearly be distinguished (Fig. 4 C), and ungrouped cases were also classified.

Length and aperture frequency distribution

The frequency distribution of fracture lengths is one of the most important numerical features of a fracture network (M.Tóth and Vass, 2011) and is usually different for different rock types in a reservoir. Therefore, the length frequency distribution was measured separately for brecciated and non-brecciated limestones. Based on these measurements, brecciated limestones have a smaller number of fractures than non-brecciated limestones but the fractures have the same frequency distribution (Fig. 4 B/5). E (elongation)

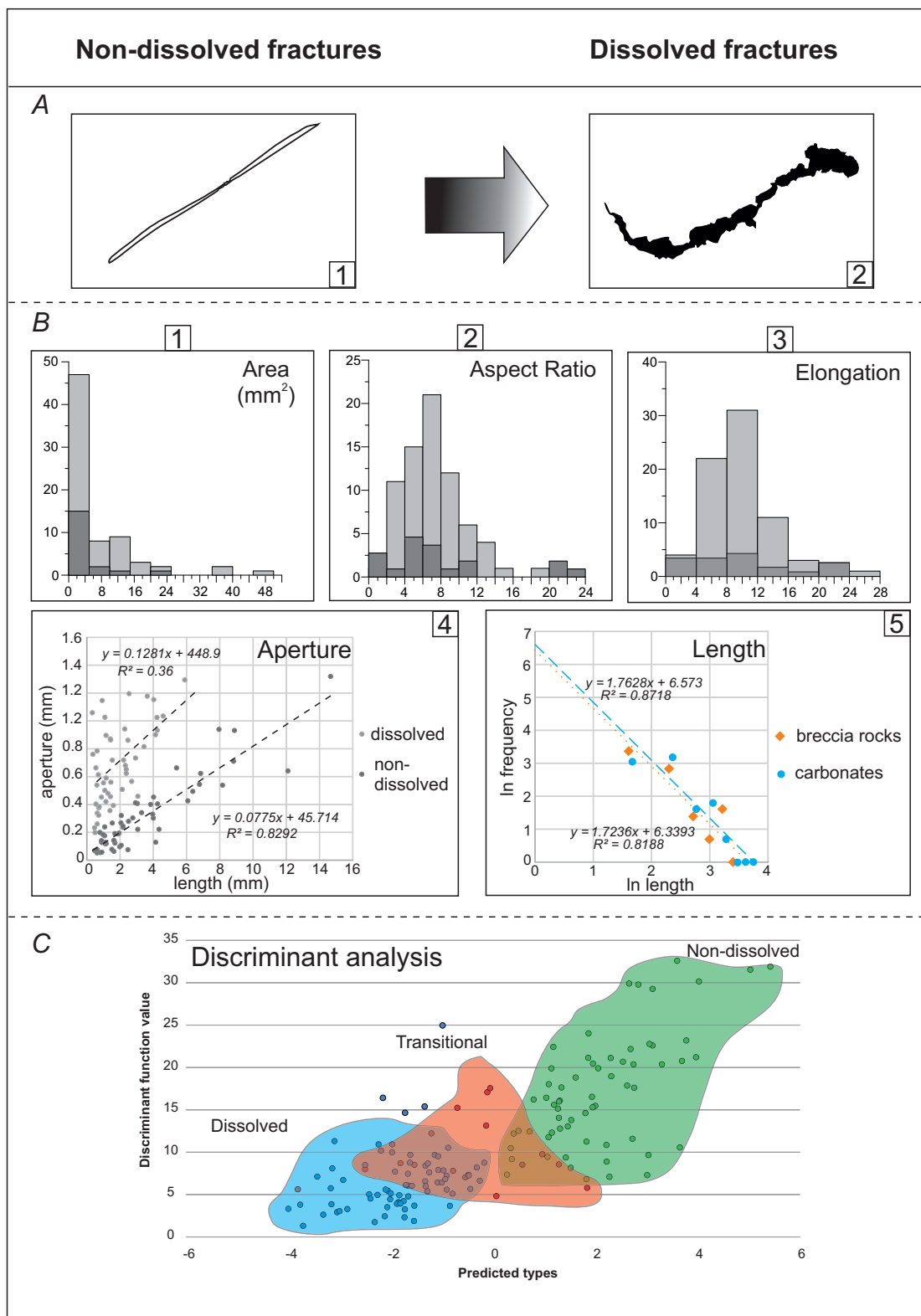


Fig. 4. Results of the individual fracture geometry measurements.

(A) Examples of dissolved and non-dissolved fracture shapes.

(B) Histograms of the main geometric parameters (B1, B2, B3); light-grey bars represent dissolved fractures, dark-grey bars represent non-dissolved fractures. **(B4)** Cross-plot showing aperture versus length relationship for dissolved and non-dissolved fractures. **(B5)** Cross-plot showing fracture length versus frequency distribution for brecciated limestones and non-brecciated samples.

(C) Graph showing the results of discriminant analysis; the green-coloured field represents non-dissolved fractures, blue represents dissolved fractures, and red represents “transitional” fractures (neither dissolved nor totally non-dissolved).

Table 2. Analysis of data from the two fracture types (dissolved and non-dissolved).

<i>Non-Dissolved</i>		<i>Dissolved</i>	
Mean	301.51	Mean	723.82
Std. Deviation	34.51	Std. Deviation	42.20
Median	221.92	Median	680.07
Variance	255.98	Variance	312.99
Skewness	42471.00	Skewness	-0.58
Kurtosis	1.83	Kurtosis	0.41
Range	1266.80	Range	1273.95
Minimum	52.35	Minimum	198.18
Maximum	1319.15	Maximum	1472.13
N	55.00	N	55
Confidence intervall (95.0%)	69.20	Confidence intervall (95.0%)	84.61

Table 3. Values of D and E (the exponent of length distribution and the fractal dimension) used for the DFN modelling at the Gomba-1 and -3 boreholes. See text for details.

Borehole: Gomba-1			Borehole: Gomba-3		
<i>Depth interval (m)</i>	<i>D</i>	<i>E</i>	<i>Depth interval (m)</i>	<i>D</i>	<i>E</i>
2475-2500	1.75	-1.7	2490-2510	1.00	-1.1
2500-2525	1.70	-1.7	2510-2530	1.10	-1.7
1525-2550	1.50	-1.7	2530-2550	1.90	-1.7
2550-2575	1.42	-1.7	2550-2570	1.45	-1.7
2575-2600	1.23	-1.7	2570-2590	1.72	-1.7
2600-2625	1.10	-1.7			
2625-2650	1.38	-1.7			
2650-2675	1.62	-1.7			

values for the brecciated and non-brecciated limestones are similar: -1.76 and -1.72, respectively.

The aperture distribution is significantly different for dissolved and non-dissolved fractures (Fig. 4 B/4). The average aperture of non-dissolved fractures is 0.30 mm while that for dissolved fractures is 0.72 mm (Table 2). Regression lines between aperture and length for both fracture types are shown in Fig. 4 B/4. The slopes of these lines are similar for dissolved and non-dissolved fractures, but the dissolved fractures have higher and more scattered values. Moreover, the trend computed for the dissolved fractures via linear regression does not intercept the Y axis at the origin, illustrating the role of dissolution.

Reservoir scale results

FMI data representing brecciated and non-brecciated zones were available from two wells, Gomba-1 and -3. The data-set includes more than 300 individual fractures in each well which could be transformed to point series for mathematical treatment (M.Tóth, 2010). The data sets show that the spatial distribution of the fracture density is heterogeneous and can be characterized by different values of the fractal dimension (D) for different depth intervals. Fracture density parameters for DFN modelling were calculated

every 25 m along the wells. The exponent of length distribution (E) and the fractal dimension (D) for the 25 m intervals are summarized in Table 3. The relationship between aperture and length was $0.124 \cdot L + 728$ for the dissolved fracture model, and $0.077 \cdot L + 45$ for the non-dissolved fracture model (c.f. Fig. 4 B/4).

Based on previous microstructural evaluations (Bauer *et al.*, 2015), four fracture generations are recognized in the study area, and these fractures may have different orientations. Although the proportions of fractures associated with each generation is not known, the FMI data sets can be used to check whether there is any variability in fracture dip direction and dip angle along the two well paths. Although there is no significant variation in dip direction, dip angle varies widely (Fig. 5). In some depth zones, fracture dip angles show little variation (with values close to zero), while high values at other depths suggest chaotic behaviour in fracture orientation (Fig. 5).

There are also particular zones in which the dip angle changes significantly. In the Gomba-1 well, significant changes in the density and calliper log data occur at depths of ~2560–2570 m; total mud loss occurred at ~2620 m; the total gamma response increases and the density decreases at 2640 m; and total mud loss and a fall in the drill bit occurred at

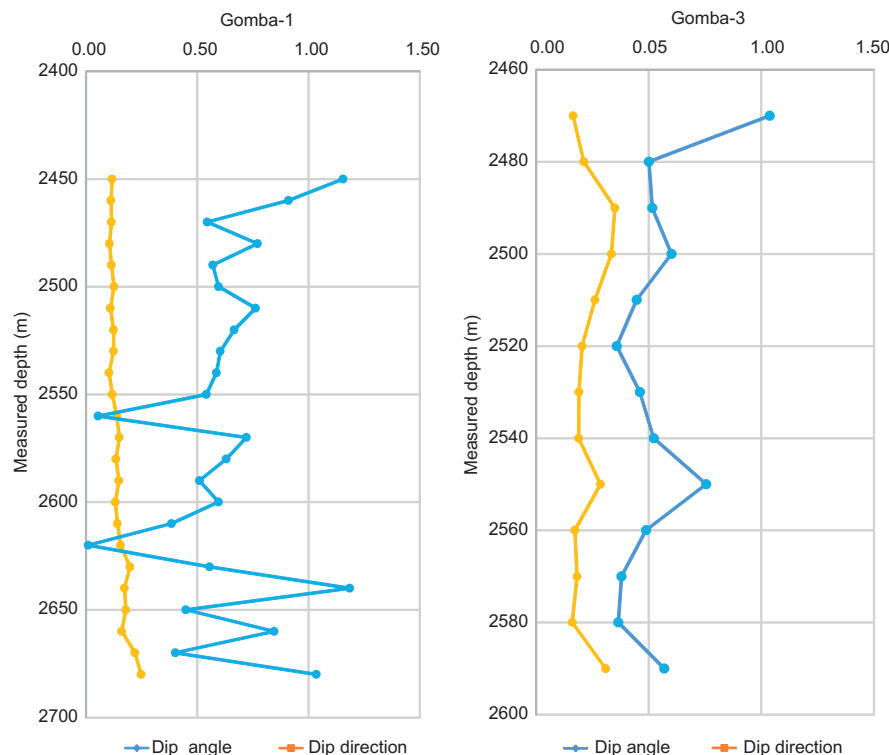


Fig. 5. Diagrams showing the downhole variation in fracture dip angle and dip direction at wells Gomba-1 and -3 (based on FMI/CBIL log data) (see Fig. 2).

2680 m (see Fig. 2). For well Gomba-3, there is a marked positive permeability anomaly at a depth of 2500 m, and the gamma log response increases, and the resistivity and neutron density decrease, at 2540–2560 m.

Fracture network simulation

Based on the characteristics of the individual fractures, two types of models were computed for the rock volumes surrounding the Gomba-1 and -3 boreholes. The first model was constructed to represent the fracture network prior to dissolution during karst-related processes; a second model was constructed to account for the effects of dissolution. The main input parameters (E, D, dip and dip direction) were the same in both cases, but the non-dissolved model used the aperture function calculated for the non-dissolved individual fractures, and the post-karstic model used the dissolved aperture function (Fig. 4 B/4). Simulations were run for a 100 m * 100 m area surrounding each well and were repeated ten times in order to analyze the model uncertainty. For both wells, the simulated fracture length interval was 1–10 m. The final DFN model consists of ~370,000 individual fractures in the case of well Gomba-1 and ~100,000 fractures in the case of Gomba-3.

An important feature of fracture networks is how coherent they are, and how many fractures define the connected sub-systems. This feature can be characterized by the size distribution of the

communicating fracture groups. In the case of the Gomba-1 well, the size distribution is asymmetric based on the model results (Fig. 6). There are two separate zones with abundant fractures along the Gomba-1 well (Fig. 7): these occur between 2450 and ca. 2510 m (in the “upper zone”) and below 2620 m (“lower zone”). The upper fracture group contains approximately 50% of all of the simulated fractures, while the lower group contains approximately 30%. Smaller clusters of fractures occur between 2510 and 2600 m (“middle zone”).

The fracture network in the carbonates surrounding the Gomba-3 wellbore is in general similar to that surrounding Gomba-1 (Fig 7), and upper, lower and middle fracture zones can be recognized. As in Gomba-1, two large fracture groups can be defined: a group containing more than 10^5 fractures, and another containing 10^2 – 10^3 fractures. However in Gomba-3, the upper 60 m of the Triassic unit is not fractured, and only insignificant fracture groups occur in this section (~100 connected fractures). Below this zone, a large fracture group occurs and contains approximately 30% of all fractures (2535–2555 m), while at greater depth, between 2570–2590 m, another significant group contains 13% of all fractures. Between these two highly fractured zones, only small fracture groups appear.

Another important feature of a stochastically simulated fracture network is the stability of the size distribution and the locations of the largest groups during repeated simulations. For both wells, ten

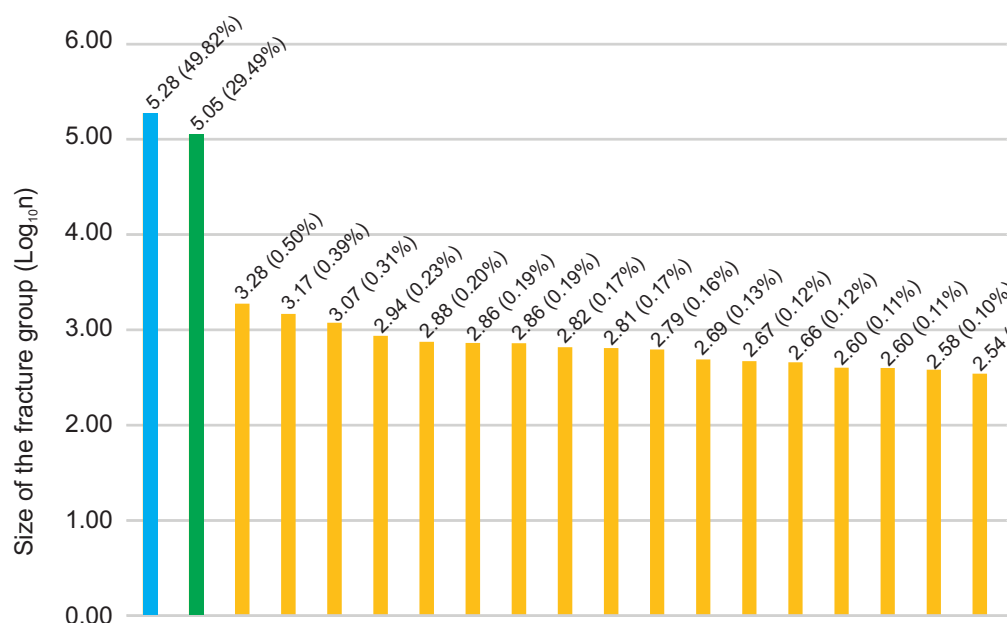


Fig. 6. Size distribution of the simulated fracture groups in the Gomba-1 well (n = the number of connected fractures in a fracture group). The total number of fractures is 378,000. The blue column represents the largest fracture group which is in the “upper zone” (Fig. 7); the green column represents the large fracture group in the “lower zone”; and the orange columns represent the intervening “middle zone” near the two larger fracture groups.

independent model runs resulted in essentially identical outputs, demonstrating that the fracture group structure is stable.

DISCUSSION

The detailed geometrical analyses showed that many of the fractures show signs of dissolution (e.g. an increase in area and convexity). Dissolution of fractures was independent of lithology; it occurs in similar proportions in both the breccia and the limestone samples, even though the breccia consists mostly of limestone fragments with a matrix is composed of both carbonate and silicate minerals. The DFN models based on quantitative data (length distribution, aperture, fracture density) and fracture orientation (dip angle and dip direction) point to the presence of three different fracture zones in wells Gomba-1 and -3 (Fig. 7). Thus an upper zone contains numerous fractures which form a single connected fracture network. The underlying middle zone contains very few fractures which do not form a coherent system and instead, small, separate fracture groups are present. Finally a lower zone consists of a large number of individual fractures which form a major interconnected fracture network. In addition there are also numerous small groups of fractures which do not however form a geometrically permeable, coherent fracture systems.

The results of this study show that the fracture network at the Gomba field is heterogeneous. In the case of the Gomba-1 borehole, the depth zones 2452–2520 m and 2620–2680 m are more highly fractured

than the other intervals. At depths of approximately 2450 m, 2570 m and 2640 m, the dip angle is highly variable (c.f. Fig. 5), suggesting a large scatter of fracture orientations. In other intervals (2540–2620 m), there is little or no variation, suggesting near-parallel fractures. In both of these cases, fracturing processes appear to be independent of the local palaeo stress field, and the highly variable fracture orientations may indicate the presence of karst-related breccia, while parallel fractures probably suggest cave roof collapse.

Previous studies of Gomba field suggest that several dissolution events have influenced the storage capacity of the carbonate reservoir rocks (Bauer *et al.*, 2016), and resulted in the formation of dissolved fractures. This effect can be identified from the fracture geometry. While the non-dissolved fractures are elongated and have small apertures, dissolved fractures usually have a more complicated and asymmetric shape (Fig. 4 A). The two groups can be distinguished using other geometric parameters (Fig. 4 C). Applying the discriminant function (equation 3) to the longest continuous core section (Gomba-1, 2492–2498 m) shows that even in a highly fractured section of the reservoir, the proportion of dissolved and non-dissolved fractures is variable (Fig. 8).

Although apertures increase, the fracture length frequency distribution does not change as a result of dissolution and follows a typical power-law function, with the same parameters for both fracture groups. As a result of dissolution, the strong correlation between aperture and length disappears; the correlation coefficient between length and aperture is weak (0.36)

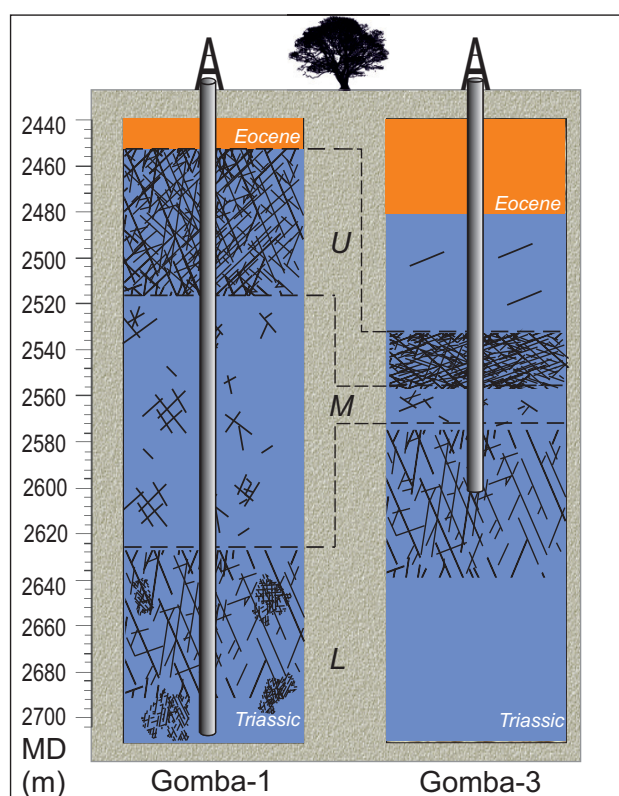


Fig. 7. Cartoons showing the results of the DFN models for wells Gomba-1 and -3. The fracture networks in the two boreholes in general follow the same patterns: a large coherent fracture group is present in the “upper zone” of the modelled interval (U); below this is a weakly fractured zone with fewer and more isolated fracture groups (M); and beneath is a zone (“lower zone”, L) in which there is a second, relatively large fracture group. There are also medium-sized fracture groups which do not create an interconnected fracture network. (U: upper zone, M: middle zone, L: lower zone).

with an anomalously large a/L ratio ($1.2 \cdot 10^{-1}$), while the corresponding values for non-dissolved fractures are 0.82 and $7 \cdot 10^{-2}$.

The studied area underwent initial burial along the main structure lineaments during the middle Eocene (Csontos and Nagymarosy, 1998). This process, together with the Mesozoic deformation phases and the Cenozoic reactivation of Mesozoic faults, created the microfracture system which was simulated by the DFN models.

According to earlier studies (e.g. Bauer *et al.*, 2015), the main geometric factor in cave formation is fracture network connectivity and not solely the number of individual fractures. Based on the above DFN model (c.f. Fig. 7), it is not likely that cave systems could form between 2520 m and 2620 m in the Gomba-1 well, or between 2475–2530 m and 2550–2570 m in the Gomba-3 well, because the fracture system is not sufficiently well-developed to allow the migration of large volumes of karst-related fluids. By contrast, the modelled upper and lower zones are likely to have well-developed cave systems. This is also suggested by the total mud loss which was recorded at 2680 m and the fact that the drilling tool was blown-off between 2679 and 2681 m (yellow stars and red star in Fig. 2a), both of which indicate the presence of open voids.

A significant proportion of the non-dissolved fractures had apertures of up to 5–10 mm which, in addition to fracture connectivity, is a fundamental requirement for cave formation (White, 1988).

As the area was exhumed during the Paleogene (Kecskeméti, 1998; Less, 2005), the karstified rocks came into contact with aggressive meteoric fluids. As a consequence, the presence of the fracture network in the upper and lower fractured zones resulted in the formation of large-scale caves and the transport of surface sediments into the fracture network.

The chaotic-textured brecciated intervals recorded within the Triassic carbonates are possible further proof of karstification. A similar lithology was interpreted as an allochthonous cave sediment by Osborne (2001). These sediments are present at particular depth intervals in both of the wells studied (e.g. in Gomba-3: 2570–2575 m, 2580 m), and are interpreted to indicate the positions of palaeo-caves. The presence of caves is also supported by the presence of freshwater limestone fragments in the breccia (e.g. Gomba-1, 2492 m; Bauer *et al.*, 2016), which are a result of CaCO_3 dissolution and re-precipitation. Fragments of freshwater limestone appear in the fine-grained matrix of the breccia.

The breccia also contains substantial amounts of dickite (Bauer *et al.*, 2016), the high-temperature polymorph of kaolin. Kaolinite is a common mineral in karstic soils and cave sediments, and develops as a result of the weathering of clay minerals in surface soils in tropical climates. These observations together suggest that sediments from shallow intervals infiltrated into the palaeocaves and were there preserved, a process characteristic of epigene karstification.

Table 4. Relationships between the DFN models, wireline log data, drilling data, FMI/CBIL log data, and the presence of cave sediments or caverns in wells Gomba- and Gomba-3.

Gomba-1					
Depth (m)	Model type	Log and drilling data	Fracture dip angle relative variation	Breccia or cavern	paleocave?
2450	Coherent	Low TG, low resistivity, high density	High	Yes	Karst related Unconformity
2560 - 2570	Isolated	High caliper, low density and resistivity	Low	Not known	NO
2620	Coherent	Total mud loss	Low	Not known	YES
2640	Coherent	High TG, low resistivity, low density	High	Not known	YES
2680	Coherent	Total mud loss, Drilling bit blows off	High	Yes	YES

Gomba-3					
Depth (m)	Model type	Log and drilling data	Fracture dip angle relative variation	Breccia or cavern	paleocave?
2475	Isolated	Low TG, low resistivity, high density	High	Not known	Karst related Unconformity
2540- 2550	Coherent	High TG, low resistivity and density	High	Not known	YES
2555- 2570	Coherent	High TG, low resistivity and density	Low	Yes	YES

In fractured and karstified rock bodies, only a small portion of the pre-existing void system is in general preserved after burial and the related collapse. In collapsed caves, a “core zone” which represents the former cave and the infiltrated sediments develops (Loucks, 1999). This is surrounded by a “disturbed zone” where bedding in the host rock is recognizable but in which numerous fractures are present. Based on the FMI data, the two most fractured depth intervals in well Gomba-1 contain significant variations in individual fracture orientations. The average dip direction of the Upper Zone is 157° , whereas that of the Lower Zone is 219° ; dip angles are 54° and 61° , respectively. Fig. 5 shows that the dip angles and dip directions vary significantly in particular zones. Fractures in most of these zones are characterized by chaotic orientations which are not consistent with a single fracture generation. Rather, they can be interpreted as a fracture system associated with the “disturbed zone” facies of Loucks (1999).

In the Gomba-1 well, there are two depth intervals with significant anomalies in fracture orientation, both of which are observable on the master log (*unpublished data from MOL plc*). In the upper interval (2560 m), the caliper log values increase, and the CDL (density) and RMLL (resistivity) values strongly decrease

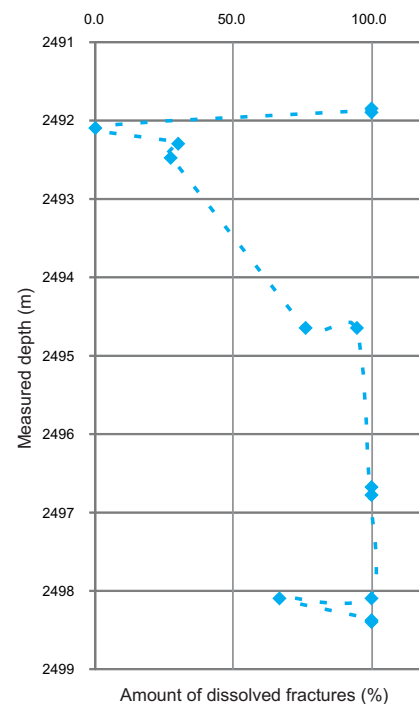


Fig. 8. Graph showing the variation with depth of the proportion of dissolved and non-dissolved fractures in the longest continuous core section in the Gomba-1 well, based on the discriminant function in equation 3.

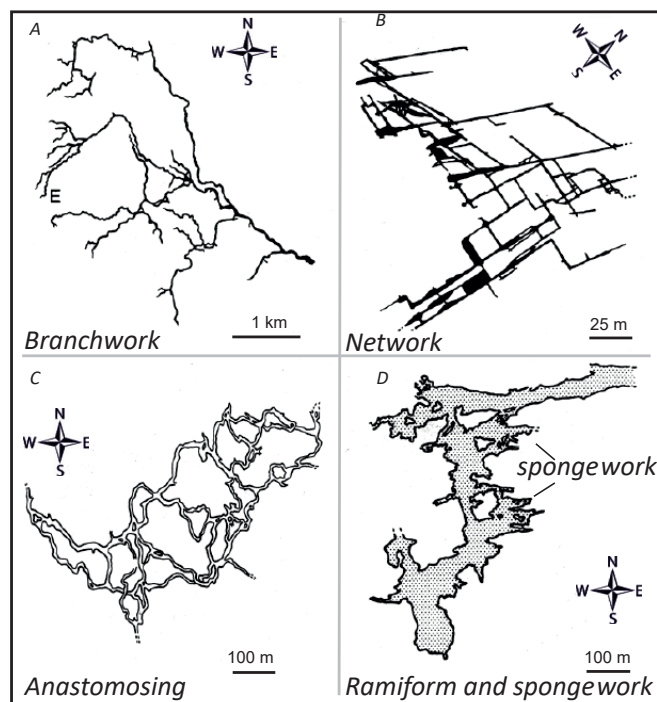


Fig. 9. Schematic diagrams showing the four fundamental cave morphologies (based on Palmer, 1991). Approximately 57% of caves are branchwork systems which are characterised by the presence of one or more sinkholes. Aggressive fluids can penetrate the karst carbonates at discrete points. Large rooms only form at the intersections of passages where cave-collapses and cave sediments frequently occur.

(Table 4). Based on the DFN models, a palaeo-cave is not assumed to occur at this depth interval. Instead, the well-log anomalies relate to an isolated fracture group. In the lower interval (2680 m), the wireline logs do not show significant anomalies but significant mud loss was observed during drilling, a clear sign of high porosity.

Based on Table 4, the presence of a palaeo cave system is predicated to occur below 2620 m in the Gomba-1 well and below 2540 m in the Gomba-3 well. The structural position and thickness of the upper fractured zone in the Gomba-1 well are similar to those in Gomba-3, suggesting the occurrence of a near-surface palaeo cave system. The breccia horizon drilled at the top of the fractured upper zone of the Gomba-1 well (Fig. 7) probably formed due to surface-related karst processes (Bauer *et al.*, 2016), following exhumation of the cave system due to erosion. Karst caves evolve in fractured rocks (e.g. Palmer, 1991; Diabat, 2013), but the spatial appearance of the caves may be very different (White, 1988; Palmer, 1991).

Modern cave geometries were classified into four main categories by Palmer (1991): branchwork, network, anastomosing, and ramiform and spongework (Fig. 9). Palmer (*ibid.*) noted that the majority (approximately 57%) of caves are of branchwork type with characteristics including vertical extents of hundreds of metres, lengths of $\sim 10^5$ m, the presence of dripstone and other speleothem deposits, and the infiltration and accumulation of surface sediment

of varying grain sizes. In the present study, the fragments of laminated fresh-water limestones and the fine-grained sediments are interpreted to result from epigene karstification. Based on these observations, it is likely that the palaeo-cave system in the Gomba field had a branchwork pattern. Although the presence of epigenetic sediments is characteristic of both branchwork and anastomosing cave types, the branchwork type is much more frequent.

The most typical characteristic of branchwork type caves is the presence of well-defined recharge zones (sinkholes), the spatial locations of which are influenced by the surface morphology and the fracture system of the country rocks (e.g. Bauer and M.Tóth, 2015). Recharge and leakage zones are more likely to develop along well-connected fracture systems than in non-fractured areas. Conduits of various sizes may develop between recharge and leakage areas. During the evolution of the cave system, each first-order branch serves as a conduit for fluids fed by a discrete recharge source, and fluid flows converge into high-order passages which become fewer and generally larger in the downstream direction (Palmer, 1991). Major structures (e.g. faults) control the directions of the high-order passages.

The spatial distribution of open voids and collapsed zones are not random, but are remnants of palaeocaves and are therefore aligned with structural trends. In the studied case, the strike of the main structural lineaments is NE-SW; hence, the collapsed zones of

the palaeo-cave system intersected by the well bore probably extend in this orientation. Although the fracture groups are geometrically isolated in both modelled wells, they are probably part of the same system. Thus, the highly fractured zones throughout the reservoir may be better hydraulically connected in a NE-SW direction than in other directions.

Unfortunately, there is not enough data to determine the precise age of the karstification. However, it is likely that the epigene karst phase began during the Paleocene, when the Mesozoic succession was exhumed. Hydrocarbon generation started only ~5 million years ago (Benedek, 2009) in response to subsidence and burial of the source rock. The presence of an extended palaeocave system in the study area may indicate the occurrence of karst-related traps for hydrocarbons. These could be related to the modelled coherently fractured zones which represent the palaeocave system, and also the unconformity at the Triassic – Eocene boundary which probably corresponds to an exhumed branch of the cave system. In addition, small isolated caverns may be present in less fractured zones which are not part of the communicating reservoir. Palaeocave systems and collapse features with high primary porosity cave sediments probably occur below 2600 m in well Gomba-1, and below 2540 m in well Gomba-3.

CONCLUSIONS

Reservoir rocks in the Gomba field (Hungarian Paleogene Basin) include fractured Triassic limestones which have been modified by karst-related processes. Based on image analyses of thin sections from cores, individual fractures show complex geometries. Fractures can be classified into two classes: one class has large 2D areas (in thin section), large apertures, complicated shapes, low elongation values, and low aspect ratios. The members of the other class have relatively high elongation values and high aspect ratios, and have simple shapes and low aperture values. The first class is interpreted to consist of dissolved fractures, and the second of non-dissolved fractures.

From FMI and CBIL log data, depth zones in wells Gomba-1 and -3 were identified in which fracture dip direction becomes chaotic or by contrast strikingly uniform. These zones are interpreted as palaeokarst zones. Based on 2D thin section data and the FMI/CBIL log information, DFN models were computed for the volumes surrounding the two boreholes. These models show that the fractures do not form a coherent network through the reservoir. Instead, upper and lower fracture systems are differentiated, but there is no connection between them.

Studies of the morphology of modern cave systems indicate that the discrete fracture groups likely formed

a branchwork type cave with a NE-SW orientation. In this orientation, the modelled fracture groups at the two wells were probably connected by dissolution and cave formation.

ACKNOWLEDGEMENTS

The authors would like to thank MOL Plc for providing the core material, thinsections, reports and the wire log data that were essential for this research. Comments by Michael Welch (DTU) and Andrew Horbury (*Cambridge Carbonates*) on a previous version of the paper are acknowledged with thanks.

REFERENCES

- BAUER, M. and M. TÓTH, T., 2015. Modeling microfracture geometry to the assess the function of a karst system (Vízfő spring catchment area, Western Mecsek Mountains, Hungary). *Geologica Croatica*, **68**(4), 11–23.
- BAUER, M., M. TÓTH, T., RAUCSIK, B. and GARAGULY, I., 2016. Petrology and paleokarst features of the Gomba hydrocarbon reservoir (central Hungary). *Central European Geology*, **59**(1–4), 28–59.
- BEAN, C.J., 1996. On the cause of 1/f-power spectral scaling in borehole sonic logs. *Geophysical Research Letters*, **23**, 3119–3122.
- BEAR, J., 1972. Dynamics in porous media. Elsevier, New York.
- BENEDEK, L., 2009. Gomba mező geológiai újrafeldolgozása és művelési terve. Mol Int. Report.
- BENKOVICS, L., OBERT, D., BERGERAT, F., MANSY, J. L. and DUBOIS, M., 1999. Brittle tectonics and major dextral strike-slip zone in the Buda karst (Budapest, Hungary). *Geodinamica Acta*, **12**(3–4), 201–211.
- CSONTOS, L., NAGYMAROSY, A., HORVÁTH, F. and KOVÁCS, M., 1992. Tertiary evolution of the Intra-Carpathian area: a model. *Tectonophysics*, **208**, 221–241.
- CSONTOS, L. and NAGYMAROSY, A., 1998. The Mid-Hungarian line: a zone of repeated tectonic inversions. *Tectonophysics*, **297**(1–4), 51–71.
- DERSHOWITZ, W.S. and EINSTEIN, H.H., 1988. Characterizing rock joint geometry with joint system models. *Rock Mechanics and Rock Engineering*, **1**, 21–51.
- DIABAT, A., AHMAD, F., HAMMOURI, N. and OBEIDAT, M., 2015. Karst development related to extensional fracture network at Bary-Kanana area, northern Jordan. *Arabian Journal of Geosciences*, **8**, 4999–5014.
- DOLTON, G. L., 2006. Pannonian Basin Province, Central Europe (Province 4808) – Petroleum geology, total petroleum systems, and petroleum resource assessment. *U.S. Geological Survey Bulletin*, **2204**(B), 47.
- FENG, K., CAO, J., HUA, K., PENG, X., CHEN, Y., WANG, Y. and WANG, M., 2013. Dissolution and its impacts on reservoir formation in moderately to deeply buried strata of mixed siliciclastic and carbonate sediments, northwestern Qaidam Basin, northwest China. *Marine and Petroleum Geology*, **39**, 124–137.
- FERET, L. R., 1931. La Grosseur des Grains des Matières Pulverulentes. *Association Internationale pour l'Essai des Matériaux*, **2D**, 428.
- FODOR, L., MAGYARI, Á., KÁZMÉR, M. and FOGARASI, A., 1992. Gravity flow dominated sedimentation on the Buda paleoslope (Hungary): record of Late Eocene continental escape of the Bakony unit. *Geologische Rundschau*, **81**(3), 695–716.
- FODOR, L., JELEN, B., MÁRTON, E., SKABERNE, D., CAR, J. and VRABEC, M., 1998. Miocene-Pliocene tectonic evolution of the Slovenian Periadriatic Line and surrounding area –

- implication for Alpine Carpathian extrusion models. *Tectonics*, **17**(5), 690–709.
- GABROVSEK, F. and DREYBRODT, W., 2001. A model of the early evolution of karst aquifers in limestone in the dimensions of length and depth. *Journal of Hydrology*, **240**, 206–224.
- GÉCZY, B., 1973. Plate tectonics and paleogeography in the East-Mediterranean Mesozoic. *Acta Geologica Hungarica*, **17**, 421–428.
- HAAS, J., BUDAI, T., CSONTOS, L., FODOR, L., and KONRÁD, G.Y., 2010. Pre-Cenozoic geological map of Hungary 1:500 000. MÁFI, Budapest.
- HÄUSELMANN, Ph., JEANNIN, P.Y. and BITTERLI, T., 1999. Relations between karst and tectonics: the case-study of the cave system north of Lake Thun (Bern, Switzerland). *Geodinamica Acta*, **12**, 377–388.
- HEWETT, T.A., 1995. Fractal methods for fracture characterization. In: Yarus, J.M. and Chambers, R.L., (Eds): Stochastic modeling and geostatistics. Principles, methods and case studies. *AAPG Computer Applications in Geology* **3**. AAPG Tulsa, USA.
- JEANNIN, P.Y., 1990. Neotectonique dans le karst du N-O du lac de Thoune (Suisse). *Karstologia*, **15**, 41–54.
- KARAY, G.Y. and HAJNAL, G., 2015. Theory and practical implementations of modelling groundwater flow in fractured rocks. *Mérnökgeológia-Közetmechanika*, 2015, 1–10.
- KAUFMANN, G., 2003. A model comparison of karst aquifer evolution for different matrix-flow formulations. *Journal of Hydrology*, **283**(1–4), 281–289.
- KÁZMÉR, M. and KOVÁCS, S., 1985. Permian-Paleogene paleogeography along the eastern part of the Periadriatic Lineament: Evidence for Continental escape of the Bakony-Drau- zug Unit. *Acta Geologica Hungarica* **28**, 69–82.
- KÁZMÉR, M., DUNKL, I., FRISCH, W., KUHLEMANN, J. and OZSVÁRT, P., 2003. The Palaeogene forearc basin of the Eastern Alps and Western Carpathians: subduction erosion and basin evolution. *Journal of the Geological Society*, **160**, 413–428.
- KECSKEMÉTI, T., 1998. Magyarország epikontinentális eocén képződményeinek rétegtana. In: Bérczi, I. and Jámor, Á., (Eds), Magyarország geológiai képződményeinek rétegtana. MOL-MÁFI kiadvány, Budapest, 403–417.
- KÓKAI, J., 1994. Exploration history and future possibilities in Hungary. In: Popescu, B.M., (Ed), Hydrocarbons of eastern central Europe, Habitat, exploration and production history. Springer-Verlag, Berlin, 147–173.
- LESS, G.Y., 2005. Paleogene. In: Pelikán, Gy., (Ed.), Geology of the Bükk Mountains. Hungarian Geological Society, Budapest, 204–210.
- LOUCKS, R.G., 1999. Paleocave carbonate reservoirs: origins, burial-depth modifications, spatial complexity, and reservoir implications. *AAPG Bulletin*, **83**(11), 1795–1834.
- MARSAN, D. and BEAN, C.J., 1999. Multiscaling nature of sonic velocities and lithology in the upper crystalline crust. *Geophysical Research Letters*, **26**, 275–278.
- MILOTA, K., KOVÁCS, A. and GALICZ, Z. S., 1995. Petroleum potential of the north Hungarian Oligocene sediments. *Petroleum Geoscience*, **1**, 81–87.
- MIN, K.B., JING, L. and STEPHANSSON, O., 2004. Determining the equivalent permeability tensor for fractured rock masses using stochastic REV approach: method and application to the field data from Sellafield, UK. *Hydrogeology Journal*, **12**, 497–510.
- M.TÓTH, T., HOLLÓS, C.S., SZÚCS, É. and SCHUBERT, F., 2004. Conceptual fracture network model of the crystalline basement of the Szeghalom Dome (Pannonian Basin, SE Hungary). *Acta Geologica Hungarica*, **47**(1), 19–34.
- M.TÓTH, T., 2010. Determination of geometric parameters of fracture networks using 1D data. *Journal of Structural Geology*, **32**(7), 878–885.
- M.TÓTH, T. and VASS, I., 2011. Relationship between the geometric parameters of rock fractures, the size of percolation clusters and REV. *Mathematical Geosciences*, **43**(1), 75–97.
- NÁDOR, A., 1993. Paleokarsts and long-term karst evolution of the Buda Mountains, Hungary. *Bulletin de la Société Géographique de Liège*, **29**, 139–143.
- NAGYMAROSY, A., 1990. Paleogeographical and paleotectonic outlines of some IntraCarpathian Paleogene basins. *Geológický Zborník. Geologica Carpathica*, **41**(3), 259–274.
- NATH, R. and PAVUR, R., 1985. A new statistic in the one way multivariate analysis of variance. *Computational Statistics and Data Analysis*, **2**, 297–315.
- OSBORNE, R.A.L., 2001. Petrography of lithified cave sediment. *Proceeding of the 13th International Congress of Speleology*, Brasilia **1**, 101–104.
- PALMER, A. N., 1991. Origin and morphology of limestone caves. *Geological Society of America Bulletin*, **103**, 1–21.
- PALOTAI, M. and CSONTOS, L., 2010. Strike-slip reactivation of a Paleogene to Miocene fold and thrust belt along the central part of the Mid-Hungarian Shear Zone. *Geologica Carpathica*, **1**(6), 83–493.
- PELIKÁN, G. Y., 2005. Geology of the Bükk Mountains. Hungarian Geological Society, Budapest.
- POPOV, S.V., RÖGL, F., ROZANOV, A.Y., STEININGER, F.F., SHCHERBA, I.G. and KOVAC, M., 2004. Lithological-Paleogeographic maps of Paratethys - 10 maps Late Eocene to Pliocene. *Courier Forschungsinstitut Senckenberg*, Frankfurt, **250**, 1–46.
- PRIEST, S.D. and HUDSON, J.A., 1976. Discontinuity spacings in rock. *International Journal of Rock Mechanics and Mining Sciences and Geomechanics Abstracts*, **13**(5), 135–148.
- RASBAND, W.S., 1997–2006. Image J, U. S. National Institutes of Health (Bethesda, Maryland, USA). Available: <http://rsb.info.nih.gov/ij/>.
- REIMANN, T., GIESE, M., GEYER, T., LIEDL, R., MARÉCHAL, J.C. and SHOEMAKER, W.B., 2014. Representation of water abstraction from a karst conduit with numerical discrete-continuum models. *Hydrology and Earth System Science*, **18**, 227–241.
- SINGURINDY, O. and BERKOWITZ, B., 2005. The role of fractures on coupled dissolution and precipitation patterns in carbonate rocks. *Advances in Water Resources*, **28**, 507–521.
- TEZUKA, K. and WATANABE, K., 2000. Fracture network modelling of Hijiori hot dry rock reservoir by deterministic and stochastic crack network simulator (D/SC). *Proceedings World Geothermal Congress*, 2000, 3933–3938.
- VASS, I., M.TÓTH, T., SZANYI, J. and KOVÁCS, B., 2009. Az aljzati kristályos háta szerepe az Alföld fluidum áramlási és hőtranszport folyamataiban (The role of the crystalline domes of the basement in the fluid migration and thermotransport processes – In Hungarian). In: M. Tóth, T., (Ed): Magmás és Metamorf képződmények a Tiszai egységben. Geolitera, Szeged, 325–341.
- WHITE, W.B., 1988. Geomorphology and Hydrology of Karst Terrains. Oxford University Press, New York.
- YANG, H.S., KANG, J.G., KIM, K.S. and KIM, C.S., 2004. Groundwater flow characterization in the vicinity of the underground caverns in fractured rock masses by numerical modelling. *Geosciences Journal*, **8**(4), 401–413.
- YIELDING, G., WALSH, J.J. and WATTERSON, J., 1992. The prediction of small scale faulting in reservoirs. *First Break*, **10**, 449–460.